ZnO-Cu_2O core-shell nanowires as stable and fast response photodetectors

Pedram Ghamgosar[a ǂ], Federica Rigoni[a ǂ]*, Shujie You[a], Illia Dobryden[b], Mojtaba Gilzad Kohan[a], Anna Lucia Pellegrino[c], Isabella Concina[a], Nils Almqvist[a], Graziella Malandrino[c], Alberto Vomiero[a]*

[a] Department of Engineering Sciences and Mathematics, Division of Materials Science, Luleå University of Technology, 971 87 Luleå, Sweden

[b] Division of Surface and Corrosion Science, KTH Royal Institute of Technology, Sweden

[c] Dipartimento Scienze Chimiche, Università degli Studi di Catania, INSTM UdR-Catania, Viale A. Doria 6, Catania, 95125

ǂ these authors contributed equally to the work

*corresponding authors:

Federica Rigoni: federica.rigoni@ltu.se

Alberto Vomiero: alberto.vomiero@ltu.se

Key words: all-oxide NWs, core-shell NWs, self-powered photodetectors, fast photodetectors, ZnO-Cu_2O heterojunction

Abstract

In this work, we present all-oxide p-n junction core-shell nanowires (NWs) as fast and stable self-powered photodetectors. Hydrothermally grown n-type ZnO NWs were conformal covered by different thicknesses (up to 420 nm) of p-type copper oxide layers through metalorganic chemical vapor deposition (MOCVD). The ZnO NWs exhibit a single crystalline Wurtzite structure, preferentially grown along the [002] direction, and energy gap E_g=3.24 eV. Depending on the deposition temperature, the copper oxide shell exhibits either a crystalline cubic structure of pure Cu_2O phase (MOCVD at 250 °C) or a cubic structure of Cu_2O with the presence of CuO phase impurities (MOCVD at 300 °C), with energy gap of 2.48 eV. The electrical measurements indicate the formation of a p-n junction after the deposition of the copper oxide layer. The core-shell photodetectors present a photoresponsivity at 0V bias voltage up to 7.7 µA/W and time response ≤0.09 s, the fastest ever reported for oxide photodetectors in the visible range, and among the fastest including photodetectors with response limited to the UV region. The bare ZnO NWs have slow photoresponsivity, without recovery after the end of photo-stimulation. The fast time response for the core-shell structures is due to the presence of the p-n junctions, which enables fast exciton separation and charge extraction. Additionally, the suitable electronic structure of the ZnO-Cu_2O

heterojunction enables self-powering of the device at 0V bias voltage. These results represent a significant advancement in the development of low-cost, high efficiency and self-powered photodetectors, highlighting the need of fine tuning the morphology, composition and electronic properties of p-n junctions to maximize device performances.

1. Introduction

It is very appealing nowadays to exploit natural solar light radiation in high-performance optoelectronic devices, working without any external power source and prepared with non-toxic, cheap and earth abundant materials, for self-powered electronic application. Metal oxides (MOx) are a broad class of non-toxic, cheap, easy to produce and abundant materials used in numerous applications, from photodetectors[1,2], to solar cells[3–6], gas sensors[7–9] , photocatalysis[10,11], water splitting[12,13]. MOx possess peculiar electronic and optical properties such as favorable bandgap for the light absorption from the UV to the visible, up to IR spectral region, good light scattering properties, when properly shaped, and tunable electronic transport, which make them perfect candidates for optoelectronic devices[14–16].

Among the different applications, photodetection is one of the most interesting. Morphology and electronic structure of the active materials play a crucial role in determining the main functional parameters of a photodetector, such as the photoresponsivity, the time response, the stability and the possibility of self-powering[17]. Self-powered systems that can work independently, wireless, with no external power source, are very attractive in areas of application such as wireless environmental sensing or in situ medical therapy monitoring. The target photoactive materials should have high absorption coefficient as well as suitable electronic properties to induce charge photogeneration, separation and collection[17].

In the recent literature, several different materials have been used as high performance self-powered photodetectors, e.g. based on perovskites[18], graphene[19] and composite graphene/perovskite[20], graphene/ZnO/Si, using the ZnO as antireflection layer[21], reduced graphene oxide (RGO)/ZnO[22], lead zirconate titanate (PZT) film[23], CdS:P3HT microwires[24]. In other examples, MOx have been studied as UV detectors[25].The most studied MOx are Cu_2O and ZnO. Cu_2O is a p-type direct bandgap semiconductor with an energy gap E_g = 2.17 eV, which enables visible light absorption. ZnO, n-type semiconductor, has direct bandgap E_g = 3.37 eV, which limits its light absorption to the UV range.

Cu_2O/ZnO heterojunctions have been previously investigated in thin film geometry for various applications[3,26,27]. However, the limited charge transport properties (mainly of the holes in the p-type semiconductor) impairs the functionality of the final device, imposing a severe constraint on the maximum thickness of the optically active material, which results in limited light absorption and significant light losses[28]. One of the most interesting alternatives to solve this open issue is the use of 1-dimensional (1D) nanostructures, which exhibit a series of advantages, compared to their thin film counterparts[4,29]. From the electronic point of view, 1D structures (especially in their single-crystalline assembly) enable much faster charge transport, compared to mesoporous/polycrystalline films. For example Docampo et al. show that SnO_2 and ZnO nanowire-based devices exhibit light-intensity-independent transport rates of

4×10^4 s^{-1}, more than one order of magnitude higher with respect to the nanoparticle-based 3D networks[30]. From the optical point of view, a disordered nanowire (NW) assembly can act as scattering layer, inducing strong light confinement of the incident light inside the NW array, thus increasing the probability of photon absorption[31]. Among the most advanced 1D devices are optoelectronic devices composed of III-V semiconductors[32,33]. While these structures demonstrated high functionalities (included, for single GaAs nanowire solar cell, photoconversion efficiency exceeding the classical limit)[32], they are typically prepared through complex and expensive techniques like molecular beam epitaxy and other high-vacuum-based routes, which are not compatible with large-scale exploitation. MOx 1D structures, instead, can be easily prepared through scalable and market-compatible methodologies, such as hydrothermal synthesis[34,35], which has been demonstrated over the years to hold great potential for the functional 1D nanostructures of several semiconducting MOx.

In the last years researchers have been working on various optoelectronic devices based on n-type ZnO NWs covered by Cu_2O as p-type layer[22,36–39] in different nanostructured geometries[40–42]. In most of them, the ZnO NW array is embedded in a Cu_2O film, and the main limitation of hole transport is not effectively addressed, leading to no improvement compared to thin film geometry.

For this reason, here we report for the first time a core-shell all-oxide ZnO-Cu_2O NW n-p junction, in which the Cu_2O layer forms a conformal shell on top of the ZnO NW array. The rationale of this geometry for optoelectronics application is (i) the decoupling of light absorption and carrier collection pathways, (ii) the improved charge transport and collection, (iii) the enhanced light trapping (multiple reflections) and (iv) the reduced use of materials, compared to bulk/thin film geometry.

We studied self-driven photodetectors based on the n-p junction between ZnO NWs and Cu_2O layer of different thicknesses, by investigating the structural, optical and electrical properties of the device, including its electrical response in dark and under light exposure. We observed strong and fast photo-response to 1 Sun irradiation (standard air mass 1.5 global, AM 1.5G, 1000 W/m^2), fast recovery time, and stable signal at room temperature.

The present study represents a step forward on the research of novel and high performing self-powered nanoscale photodetectors based on earth abundant and sustainable materials like MOx. It demonstrates the effectiveness of modulating both the shape (through 1D nanostructuring) and structure (through tuning the thickness of the optically active layer) to boost the functionality of the end-user device.

2. Experimental methods

2.1 Synthesis

ZnO NWs have been synthesized by hydrothermal method[34] and covered by Cu_2O p-layer by metal-organic chemical vapor deposition (MOCVD). We prepared four different samples: bare ZnO NWs

(sample a), 70 nm Cu_2O on ZnO NWs (sample b), 240 nm Cu_2O on ZnO NWs (sample c) and 420 nm Cu_2O on ZnO NWs (sample d). The reported nominal thickness of the samples is based on the deposition of the copper oxide film on a Si reference substrate. For the hydrothermal synthesis of ZnO NWs, first a seed layer of ZnO was deposited on fluorine-doped tin oxide (FTO) conducting glass (Pilkington TEC 15, 15 ohm/sq) by spin coating 0.1 M of zinc acetate dihydrate in ethanol and heat treatment at 450 °C for 1 hour at ambient atmosphere. Then 100 mM of $Zn(NO_3)_2 \times 6H_2O$ and 100 mM of hexamethylenetetramine (HMTA) in water were mixed in an autoclave and the seeded substrate was placed inside. The autoclave was heated at 95 °C for 3 hours.

MOCVD was performed in a reduced pressure, horizontal, hot-wall reactor made of a silica tube from the $Cu(tmhd)_2$ (Htmhd = 2,2,6,6-tetramethylheptan-3,5-dione) precursor. The $Cu(tmhd)_2$ compound was purchased from Sigma-Aldrich and used without further purification. The reactor was evacuated with a scroll pump unit. Each section was heated independently, with ± 2 °C accuracy, using computer-controlled hardware. The total pressure, measured using a MKS Baratron 122AAX was in the range 4-5 Torr. Pre-purified Ar and O_2 were used as carrier and reaction gases, respectively. The mass flow rates were controlled using MKS 1160 flow controllers and a MKS type 247 electronic control unit.

A ZnO thin film (100 nm thick) was prepared by reactive sputtering from a ZnO target to compare with the optical response of ZnO NWs.

2.2 Characterization

Scanning electron microscopy (SEM) was performed using a field emission scanning electron microscope (FE-SEM) ZEISS SUPRA 55 VP. X-ray diffraction (XRD) patterns were acquired through a Bruker-AXS D5005 θ-θ diffractometer, using a Göbel mirror to parallel the Cu Kα radiation operating at 40 kV and 30 mA.

The optical characterizations (transmittance and diffuse reflectance) were performed by Cary 5000 spectrophotometer. Cary 5000 UV-vis-NIR spectrophotometer consists of double beam, ratio recording, double monochromator incorporating with R928 photomultiplier tube detector (PMT detector, UV-vis region), and PbS photocell detector (NIR region). It covers the 175-3300 nm range and it is equipped with different sample holder and internal diffuse reflectance accessory. The photoluminescence (PL) measurements were carried out by a high-resolution spectrofluorimeter (FLS980 from Edinburgh Instruments). Steady state PL excitation of the samples is provided by a broadband Xe-lamp in the 230-1300 nm region. The spectral detection range of the emission covers the whole UV-Visible-NIR, from 250 nm to 1700 nm. The excitation wavelength λ_{exc}=305 nm was used in our measurements.

The macro electrical measurements were performed by a source picoammeter (Keithley 2401) equipped with a solar simulator. Two brass metal screws constitute the metal contacts on top of the sample. The

Keithley can measure the voltage and current in the range of 1 μV – 21 V and 10 pA - 1 A, respectively. The solar simulator consists in a Xe lamp with an AM 1.5 - Global filter, which can generate vis-UV light with the power intensity of 1 Sun (100 mW cm^{-2}). The light intensity of the solar simulator was controlled through a calibrated silicon solar cell.

The ZnO-Cu_2O core-shell samples were tested as photo-sensors by tracking the current density-voltage (J-V) curves and the time dependent self-powered photo-response at 0 V applied bias, under 1 Sun simulated light irradiation in air and at room temperature. The light illuminated the sample from the bottom, passing through the FTO/glass substrate and then reaching the active oxide layers of the photodetector. Electrical measurements were carried out by using a picoammeter (Keithley 2410) with the working electrode in contact with the top oxide layer, and the FTO substrate grounded. In this configuration, we have reverse bias for $V < 0$ (where negative voltage is applied to the p-layer) and forward bias for $V > 0$ (where positive voltage is applied to the p-layer) in the J-V plot.

The AC impedance spectra were measured in the dark and under illumination by a Solartron XM FRA 1MHz coupled with a Modulab XM ECS, Solartron potentiostat, on samples with a surface area of 0.16 cm^2. The AC signal was 10 mV and the frequency range 1 MHz–500 Hz.

3. Results and discussion

3.1 Morphological, structural and optical properties

Figure 1 (left) shows the SEM images of bare ZnO NWs (Fig. 1a) and ZnO NWs with different Cu_2O layers (Fig. 1b-d). We obtained a homogeneous grass-like layer of NWs aligned quasi-perpendicular to the substrate, with NWs length around 1.1 μm (Inset of Fig. 1a), an average diameter of (71 ± 7) nm (see high resolution SEM in SI1 of Supplementary Information). Copper oxide deposition results in a conformal and homogeneous coverage of ZnO NWs. Different deposition parameters of the MOCVD process (reported in Table 1) result in different layer thickness, and different phase composition (see XRD data, Fig. 2). Specifically, at 250°C the copper oxide layer appears very smooth (sample b and c) with a core-shell diameter of about (110 ± 10) nm for sample b and (160 ± 10) nm for sample c. When prepared at 300°C (sample d), the roughness of the surface layer significantly increased, the core-shell structure is less evident, and a continuous film is observed. The thickness of the Cu_2O layer refers to the thickness deposited on a reference Si substrate, and roughly corresponds to the thickness deposited on the top surface of the NWs. The thickness of the Cu_2O layer deposited on the lateral side of the ZnO NW is, instead, lower, as expected. We estimated the thickness of the layer deposited on the lateral side of the NWs by comparing the ZnO NWs dimensions before and after Cu_2O deposition (data reported in Table SI1 of the supplementary information) and we visualized the situation in the sketches reported in Figure 1 (right). The diameter of the core-shell structure, compared to the ZnO NWs dimensions gives an estimated

lateral side thickness of the Cu_2O layer of about 20 nm for sample b, 45 nm for sample c and 156 nm for sample d (see SI1).

Table 1. Deposition parameters during the MOCVD process. Phase (see XRD data in Fig. 2), deposition temperature and time, vaporization temperature of the precursor and final thickness of the layer.

Sample	**Phase**	**Dep. T (°C)**	**Dep. Time (min)**	**T precursor (°C)**	**Cu_2O thickness (nm)**
(b) 70 nm Cu_2O/ZnO	Cu_2O	250	30	130	70 ± 10
(c) 240 nm Cu_2O/ZnO	Cu_2O	250	120	130	240 ± 10
(d) 420 nm Cu_2O/ZnO	Cu_2O + CuO imp.	300	120	135	420 ± 10

The underlying photo-response mechanism investigated in this work is depicted in Fig. 1e, showing the electronic band bending and the space-charge region, which provide the driving force to separate the excitons generated under illumination, at 0 V bias applied. The energy gap and the band alignment play a crucial role in the photo-response mechanism. We propose in Fig. 1e the Cu_2O-ZnO junction scheme for conduction and valence band, in agreement with the present literature in the field[43–45].

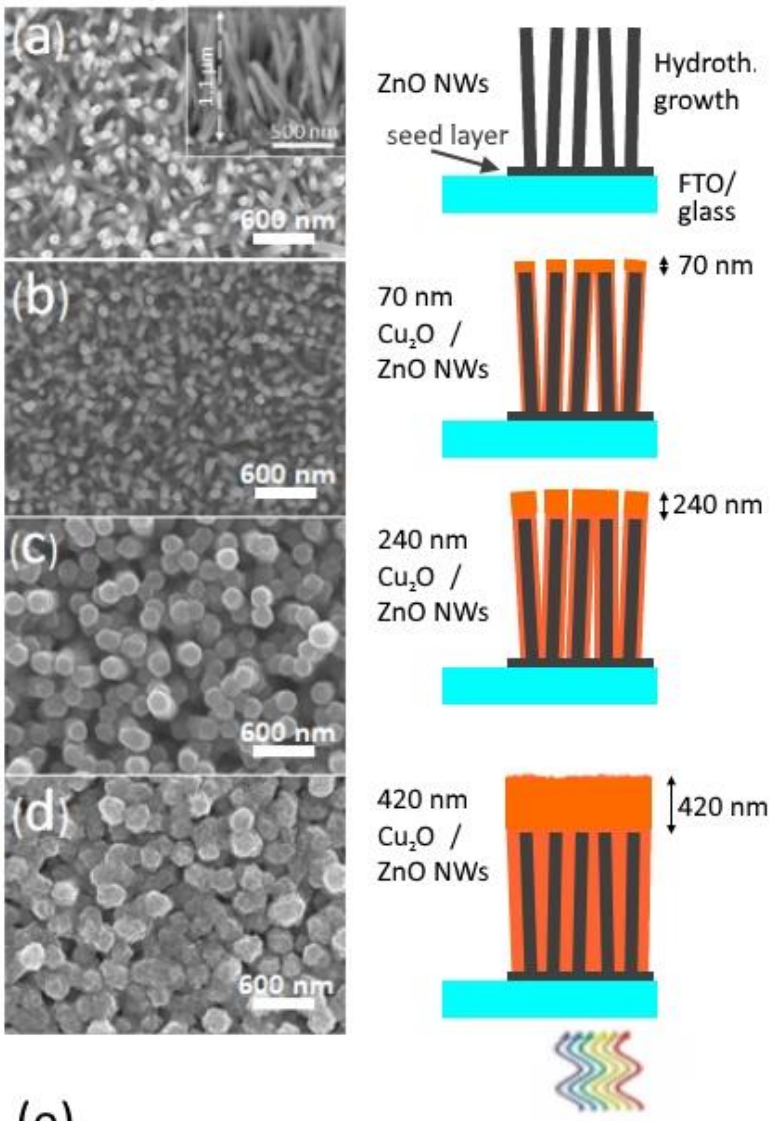
(a)
1.1 µm
500 nm
600 nm
(b)
600 nm
(c)
600 nm
(d)
600 nm
ZnO NWs
seed layer
Hydroth. growth
FTO/ glass
70 nm
70 nm Cu2O / ZnO NWs
240 nm
240 nm Cu2O / ZnO NWs
420 nm
420 nm Cu2O / ZnO NWs

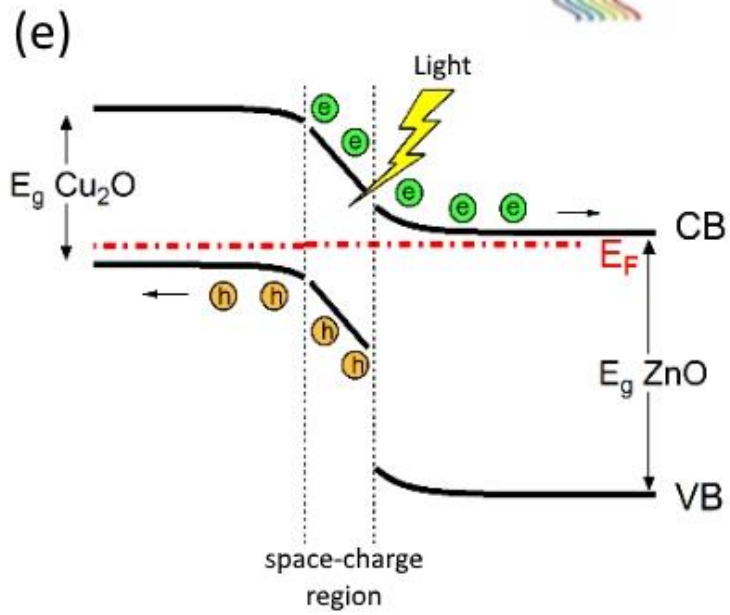
(e)
Light
e
h
Eg Cu2O
CB
EF
Eg ZnO
VB
space-charge region

Fig. 1. SEM images (left) and sketches (right) of ZnO bare NWs (a), ZnO NWs covered by 70 nm (b), 240 nm (c) and 420 nm (d) Cu_2O layer (represented by the red coverage on the grey ZnO NWs in the sketches). For the photo-detection measurements, the visible light is coming from the bottom of the sample (through the FTO/glass substrate). Energy band bending diagram of Cu_2O/ ZnO heterojunction and the self-powered photo-sensing mechanism at 0 V bias applied (e).

In Fig. 2, the XRD patterns of bare ZnO NWs and ZnO NWs covered by Cu_2O are shown. The intense (002) diffraction peak at 34.4° in the XRD pattern (Fig. 2a) confirms the preferential growth direction of single crystalline ZnO nanowires (before copper oxide deposition) with Wurtzite structure (PDF 36-1451). In this structure, which is the most thermodynamically stable, the zinc and oxygen atoms sit on tetrahedral positions.

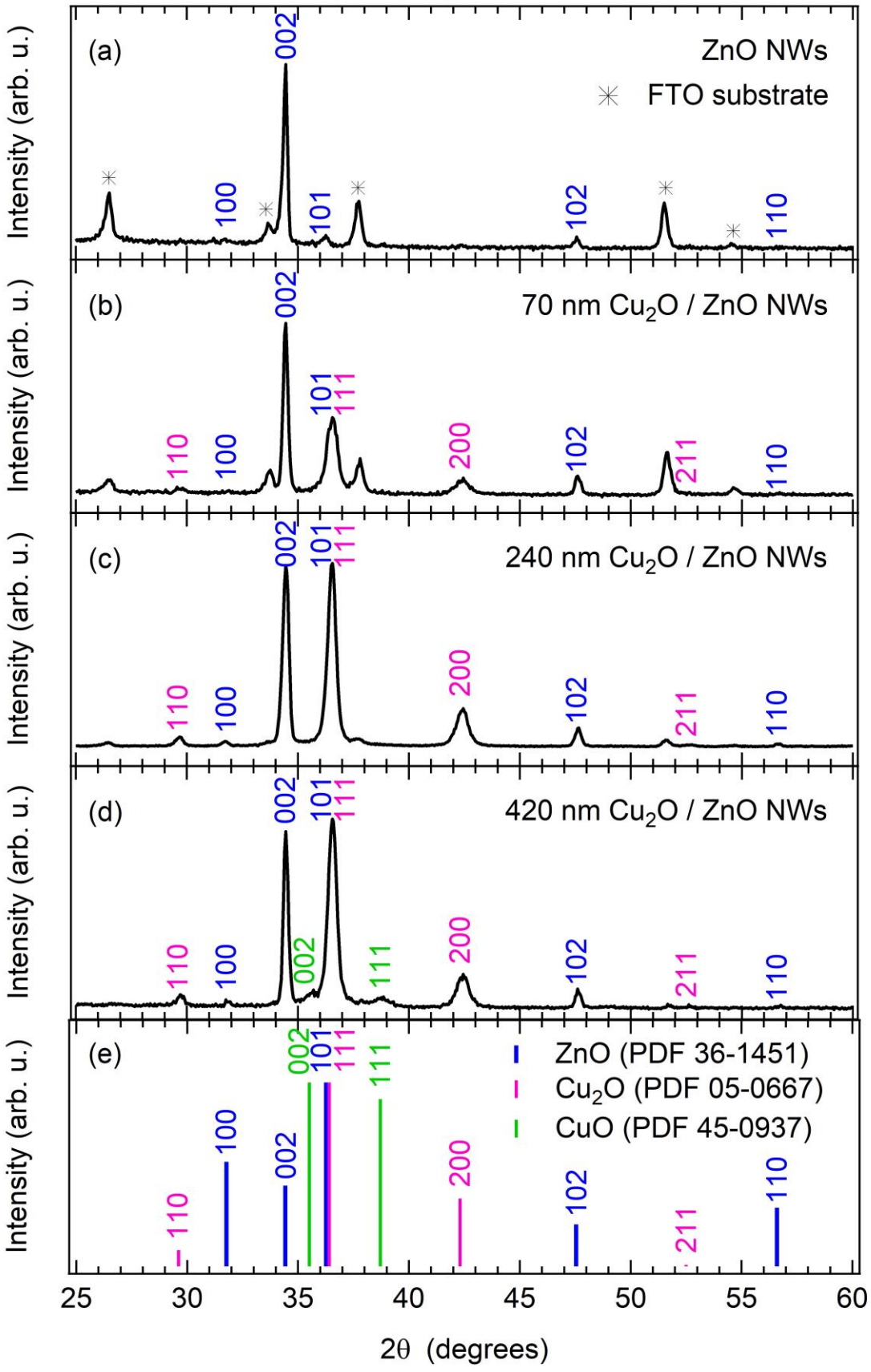
(a)
ZnO NWs
FTO substrate
(b)
70 nm Cu2O / ZnO NWs
(c)
240 nm Cu2O / ZnO NWs
(d)
420 nm Cu2O / ZnO NWs
(e)
ZnO (PDF 36-1451)
Cu2O (PDF 05-0667)
CuO (PDF 45-0937)
Intensity (arb. u.)
2θ (degrees)
25
30
35
40
45
50
55
60

Fig. 2. XRD patterns of ZnO bare NWs (a), ZnO NWs covered by 70 nm (b), 240 nm (c), 420 nm (d) Cu_2O layer. PDF reference for ZnO, Cu_2O and CuO (e).

After deposition of copper oxide, the ZnO nanowires keep the Wurtzite structure with the hexagonal unit cell, confirmed by the presence of the (002) diffraction peak also in Fig. 2 b-d. The lattice planes for Cu_2O (PDF 05-0667) are (110), (111) and (200), which show up at diffraction angles equal to 29.6°, 36.5° and 42.3°, respectively, indicating the crystalline cubic phase[46]. For the CuO (PDF 45-0937), peaks at 35.6° and 38.8° may be associated with the (-111)-(002) and (111)-(200) lattice planes, respectively[46]. In the sample grown at 250 °C (sample b and c, Fig. 2b,c) only Cu_2O phase is present for copper oxide (peaks at 29.6°, 36.5° and 42.3°), while no peak is present related to CuO. In the sample grown at 300 °C (sample d, Fig. 2d), the two typical peaks of CuO appear at 35.6° and at 38.8° diffraction angles, indicating the presence of CuO impurities. The apparently unusual formation of Cu(I) oxide using a Cu(II) precursor, without any reducing atmosphere, may be explained considering that the organic moiety acts as a reducing agent under the deposition conditions[47]. On the other hand, the temperature plays a crucial role, with low temperature stabilizing the Cu_2O vs. CuO, which appears already at 300 °C[48].

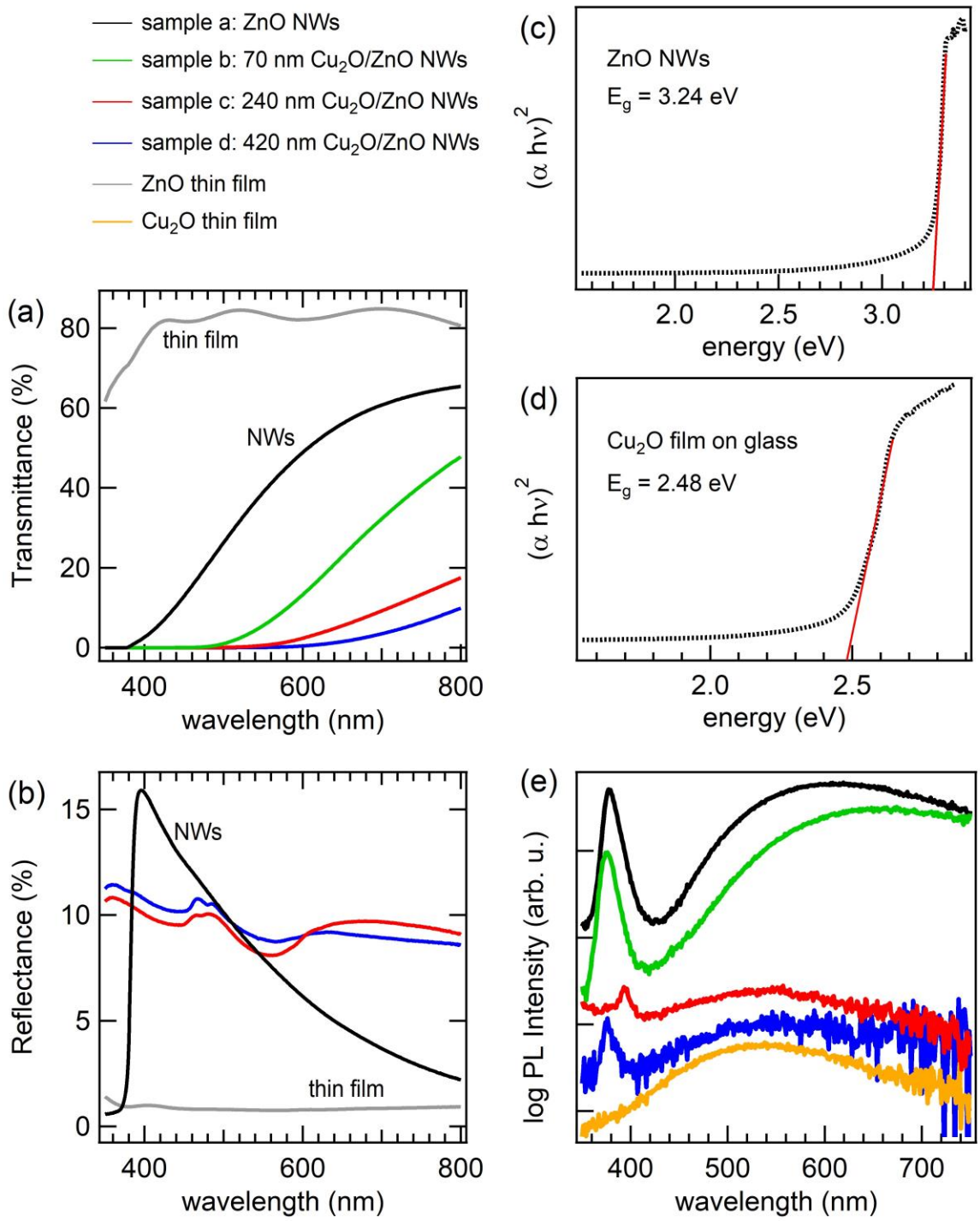

Fig. 3. Transmittance (a) and diffuse reflectance (b) spectra of the ZnO NWs and Cu_2O/ZnO NWs samples compared to ZnO and Cu_2O thin film. Tauc plot of ZnO NWs (c) and Cu_2O thin film on glass (d). PL spectra of the ZnO NWs and Cu_2O/ZnO NWs samples compared to the pure Cu_2O thin film (e).

Figure 3 shows the optical properties of bare ZnO NWs and ZnO-Cu_2O core-shell samples. In Fig. 3a, the transmittance spectra of the bare ZnO NWs, 70 nm, 240 nm and 420 nm Cu_2O layer on ZnO NWs are reported, compared with the transmittance from a ZnO thin film (100 nm). The transmission of the ZnO thin film results around 80% (calculated value 82±4.5) on average in the range 350-800 nm, while the ZnO NWs show a much lower transmission, in particular for low wavelengths. As expected, the transmittance of the ZnO covered by copper oxide samples is lower than the bare ZnO NWs, thanks to the absorption of copper oxide species in the UV-VIS-NIR range. In particular, the transmittance scales with the thickness (higher the copper oxide thickness lower the transmittance) and no transmittance is recorded for $\lambda<600$ nm (for samples c and d). The sample grown at 300 °C (sample d) shows the highest optical density, most likely due to the highest thickness, compared to the samples grown at lower temperature. An additional contribution to the increase of light absorption can be the presence of the CuO species, as highlighted by the XRD. CuO has lower energy gap (nominally, E_g ~ 1.4 eV corresponding to an absorption onset at λ = 870 nm) compared to Cu_2O (nominally, E_g ~ 2.5 eV), broadening the range of the absorbed light. The effect of scattering from the NWs is also confirmed by the diffuse reflectance, shown in Fig. 3b. ZnO thin film shows very low reflectance signal, as expected, while the diffuse reflectance from ZnO NWs is enhanced in the range 370-800 nm, with a peak of R=15.9% at 395 nm. For ZnO NWs covered by copper oxide layer (samples c and d) we observed similar diffused reflectance, around 10%, in the analyzed spectral range.

From the transmittance spectra and the Lambert-Beer law, we calculated the absorption coefficient α ($\alpha=(1/d)\times\ln(100/\%T)$, where d is the sample thickness and $\%T$ the transmittance) and the energy gap E_g, related through the Tauc expression for a direct band gap material[26]:

$$\alpha^2=A(h\upsilon-E_g)^n \quad (1)$$

Where A is a constant, $h\upsilon$ is the photon energy and n is equal to 1 for a direct bandgap material. Through linear extrapolation of the plot of $(\alpha h\upsilon)^2$ versus $h\upsilon$, i.e. the Tauc plot, the band gaps were calculated. In Fig. 3c and 3d the Tauc plot of ZnO NWs and thin film of 420 nm Cu_2O on glass substrate is reported, obtaining an optical energy gap of 3.24 eV for ZnO and 2.48 eV for Cu_2O (we observed the same optical energy gap also for the other Cu_2O thicknesses).

Photoluminescence (PL) of the samples was carried out using a λ_{exc} = 305 nm excitation wavelength laser source (Fig. 3e). In the bare ZnO NW sample, the peak at 377 nm is attributed to the near band edge emission (NBE) of ZnO NWs and the broad peak in the visible range (peaked at 600 nm) is related to ZnO surface defects in the crystalline structure[49,50]. The pure Cu_2O spectrum (orange curve) shows a broad band peaked at 530 nm, shifted at lower wavelengths with respect to the green ZnO emission. The effect of the presence of Cu_2O on top of the ZnO NWs resulted in the decreased NBE emission intensity from

ZnO and in the shifts of the visible PL emission band towards the visible emission of Cu_2O, at lower wavelength.

3.2 Electrical measurements

Figure 4a shows the J-V curves in dark and under illumination, by exposing 0.16 cm^2 of the sample to 1 Sun. As expected, the FTO substrate shows a linear ohmic behavior and no effect under light illumination was observed (light-blue lines in Fig. 4a). The bare ZnO NWs (sample a, black lines) show a rectifying behavior in the dark J-V curve and become more conductive under light illumination for both reverse ($V<0$) and forward bias ($V>0$). The rectifying behavior of ZnO sample in dark could be due to: (1) the junction with FTO, (2) the Schottky junction with the metal contact. When the sample is illuminated, it becomes more conductive and this effect overcomes the weak effect of the junction with the FTO or the metal contacts. On the other hand, ZnO-Cu_2O samples keep a rectifying behavior also under illumination, due to the presence of the p-n junction between the two oxides. By comparing the dark J-V curves of the ZnO-Cu_2O samples (solid lines in Fig. 4a), we observe that the thinner the Cu_2O layer, the lower the flowing current. The illumination increases the current density in the forward bias region for all the ZnO-Cu_2O core-shell samples (dashed lines in Fig. 4a), but the rectifying behavior in the J-V curves is still present (very low current is observed for $V<0$ even under light illumination). This rectifying behavior in the J-V curves confirms the presence of a p-n junction between the n-type ZnO NWs and the p-type Cu_2O layer. Although all the samples become more conductive under light illumination, no clear photovoltaic effect was observed in the J-V curves.

To compare the illumination effect on the different ZnO-Cu_2O samples, we analyzed the ratio between the current density under illumination, J_L, and in dark, J_D, as shown in Fig. 4b. For $V > 0$ V, samples a and d show a constant J_L/J_D ratio, while in sample b and c the ratio increases from 1 to 3.7 and from 1.5 to 3.0 at 1V, respectively (the current density of sample c at 1V results 0.2 mA/cm^2 in dark and 0.7 mA/cm^2 under light, while the current density of sample b is very low, less than 18 $\mu A/cm^2$ even under illumination). The J_L/J_D ratio overcomes the one of the other samples, however J_L/J_D is close to 1 for $V = 0$ (meaning no response to light in self-power condition). Moreover, at voltage near 0V, sample c shows not only a higher current density, but also a higher J_L/J_D ratio with respect to the other ZnO-Cu_2O sample. Sample d, instead, while showing a higher current density (0.7 mA/cm^2 in dark and 1.1 mA/cm^2 under light), presents a constant and low photoresponsivity. In fact, if on one hand a thick absorbing layer allows a high light absorption, it also results in a high series resistance, due to its low charge mobility, which affects the photoresponse performances. Indeed, a compromise is needed in the choice of the absorbing layer thickness to maximize light absorption, while keeping a low series resistances. Both from DC electrical

measurements (shown in Fig. 4) and AC impedance spectroscopy (IS), which allowed to obtain series resistance values (see Fig. 5), we can conclude that the best Cu_2O thickness in the present study is 240 nm. In Fig. 4c-f, current density versus time is reported during dark/light cycles of 10 s, at 0 V bias voltage applied to the samples. The bare ZnO NWs show very low (of the order of 10^{-2} $\mu A/cm^2$) and slow response (of the order of a few seconds) and recovery to light exposure (Fig. 4c). In Fig. 4d, sample b shows a very low current density (in the order of 10 nA/cm^2) and low response to light, but faster compared to sample a (0.36 s for the rise time and few seconds for the recovery). Samples c and d (Fig. 4e and 4f), instead, show very fast response to light as well as very fast recovery times (two orders of magnitude faster than bare ZnO in both cases) and a significantly higher photogenerated current density (one order of magnitude in both cases). Sample c (Cu_2O thickness 240 nm) also features a photogenerated current density more than three times higher (0.80 $\mu A/cm^2$ versus 0.25 $\mu A/cm^2$) with respect to sample d (Cu_2O thickness 420 nm).

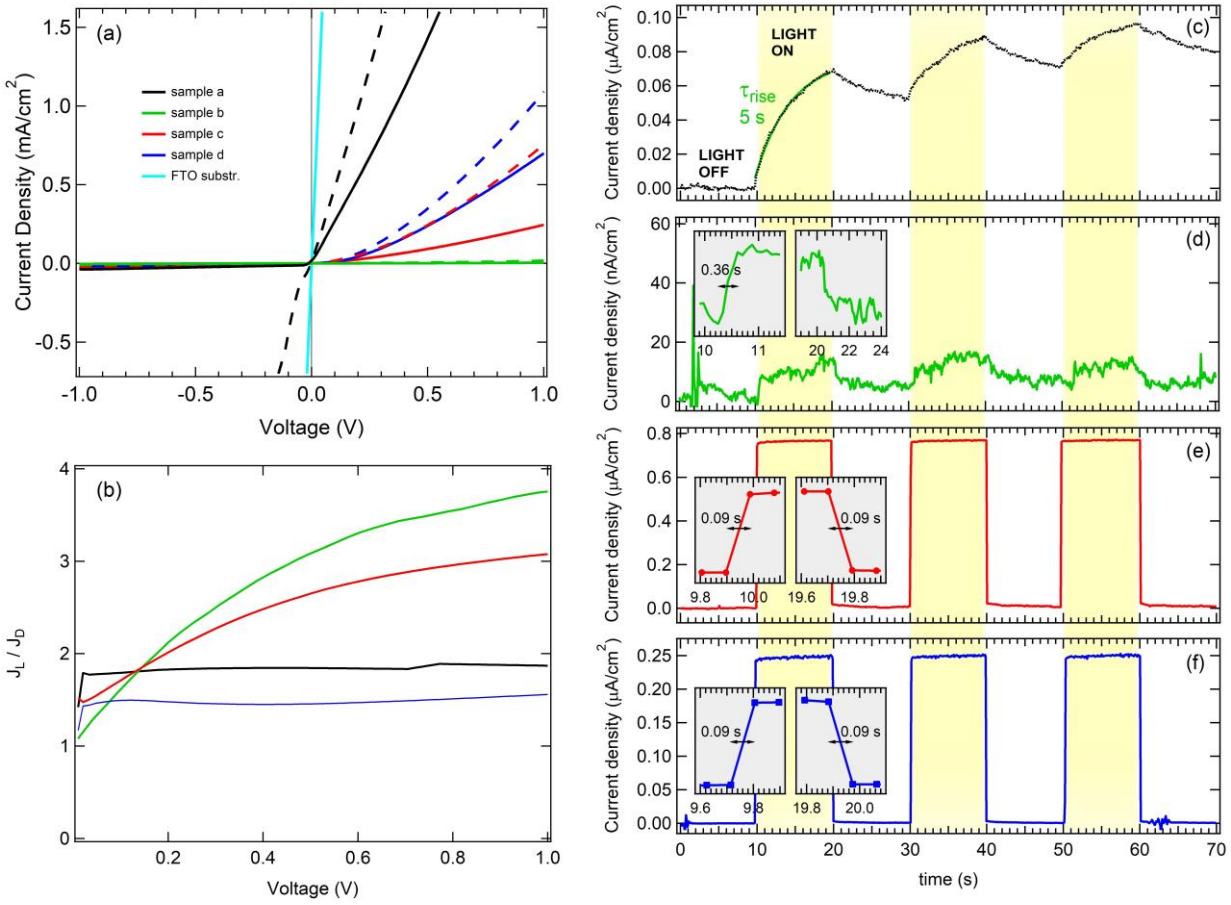

Fig. 4. J-V curves carried out in dark (solid lines) and under 1 Sun illumination (dashed lines) for the different samples (a). J_L/J_D, ratio between light and dark current density, for V > 0 V (forward bias region) (b). Current density vs time during dark/light cycles of 10 s at 0 V bias voltage applied to ZnO bare NWs sample (c), 70 nm (d), 240 nm

(e) and 420 nm (f) Cu_2O/ZnO NWs. The blow-up in the insets show the response and recovery time of the core-shell ZnO-Cu_2O NWs.

The photoresponsivity is defined as the photocurrent through the detector per active area per unit power of light[17]. Our samples were irradiated by 1 Sun (1000 W/m^2) and the photoresponsivity to visible light in terms of (current density) / (incident power density) was calculated. We obtained the following photo-response values: (0.7 ± 0.1) μA/W for sample a; (0.13 ± 0.01) μA/W for sample b; (7.67 ± 0.02) μA/W for sample c; (2.48 ± 0.01) μA/W for sample d. The enhanced photo-response of sample c may be attributed both to the strong Cu_2O contribution in the optical absorption for this core-shell ZnO-Cu_2O sample, which show a gap of 2.48 eV (see Fig. 3d) and to a suitable thickness, which keeps a low series resistance.
The combination of favorable gap and thickness enables high light absorption and reasonably low series resistance.
From the time dependent self-powered photo-response at 0 V applied bias, we analyzed the response and recovery times during 10 s dark/light cycles (shown in Fig. 4c-f). The rise curve during light exposure of ZnO bare NWs (sample a) was fitted with a single exponential function obtaining τ_{rise} = (4.7 ± 0.1) s, where τ_{rise} is the time constant of the single exponential fitting curve. The response and recovery times for this sample (defined as the time needed to reach the 90% of maximum intensity and to recover the initial intensity within 10%, respectively) are very slow, more than 10 s and more than 60 s, respectively, as shown in Fig. 4c. On the other hand, the core-shell ZnO-Cu_2O samples show enhanced response and recovery times below 0.09 s (this value represents an upper limit due to the response time of the acquisition setup). By comparing our results with other visible light oxide photodetector systems in literature (see Table 2), we obtained faster response and recovery times with respect to any visible oxide photodetector based on oxide heterojunction[1,2,51]. Faster oxide photodetectors have been previously reported[52–54] but they are limited to the UV detection range, being them based on wide band gap materials (like ZnO, TiO_2 and SnO_2). In the literature, also in all-oxide UV photodetection, the core-shell structure improves the response and recovery time of the photodetector device[53,54]. In fact, Gao et al. reported self-powered UV-photodetectors made of TiO_2 coated ZnO nanostrawberry aggregates[53] and self-powered UV-photodetectors based on ultrathin SnO_2-TiO_2 core-shell electrodes[54], showing response and recovery times faster (see values reported in table 2) than other not core-shell structures, e.g. nanocrystalline TiO_2 film self-powered UV-photodetector[52]. We can conclude that the fast response of our ZnO-Cu_2O samples, compared to the previous literature on visible oxide photodetectors, can be attributed to the core-shell structure of the p-n junction, which allows a more efficient and faster charge separation and collection.

Table 2. Response (rise) and recovery times compared with other fast response photodetectors in literature.

Response time (s)	Recovery time (s)	Structure	Material	Range of detection	Reference
≤ 0.09	≤ 0.09	Core-shell nanowires	ZnO-Cu_2O	VIS	This work
0.14	0.36	Nanowires	ZnO-Cu_2O	VIS	[51]
0.22	0.32	Cu_2O film / ZnO nanorods	ZnO-Cu_2O	VIS	[2]
~ seconds	~ seconds	Cu_2O nanoneedles / ZnO nanorods	ZnO-Cu_2O	VIS	[1]
0.08	0.03	Film	TiO_2	UV	[52]
0.022	0.009	core-shell	ZnO-TiO_2	UV	[53]
0.02	0.004	core-shell	SnO_2-TiO_2	UV	[54]

To evaluate the sample series resistance, AC IS has been carried out on the samples that showed the best photodetection response, i.e. sample c and d, and on ZnO NWs. In Fig. 5, the AC IS data for the samples in dark condition are shown in Cole-Cole plot. We cannot compare the absolute value of the different IS spectra, because the force applied by the screw on the sample surface is slightly different. However, as the set-up was the same for all the four samples, we can compare the impedance spectra shape and obtain information on the equivalent circuit. All the AC impedance spectra in dark and under light illumination are reported in the Supplementary Information (Fig. SI2).

For sample a (bare ZnO NWs), we can simulate the IS data by an equivalent circuit with a series resistance and one RC pair (Fig. 5a), i.e. by a single semi-circle. R_1 is the series resistance (R_1=R_S) and it represents the Ohmic contributions of the contacts and the device bulk and R_2 and C_1 in the RC pair represent the contribution of the ZnO seed layer at the ZnO/FTO interface, as already observed by Li et al.[55]. In this work, Li et al. performed AC impedance spectroscopy on a piezotronics device composed of a Cu layer and FTO glass sandwiched ZnO nanowires array (Cu/ZnO/FTO), by applying different forces. In all cases, they observed IS spectra which is simulated by an equivalent circuit with a series resistance and a double RC pair, i.e. double semi-circle, one related to the ZnO seed layer contribution and the other one to the metal Schottky contact between ZnO NWs and Cu layer. In contrast with Ref. 46, we did not observe a junction contribution due to the Schottky junction between the metal contact and the ZnO NWs (we can simulate the IS data by a series resistance and a single RC pair). We can conclude that in our case the contact between the metal (the screws) and the ZnO NWs shows a more ohmic than Schottky-junction like behavior.

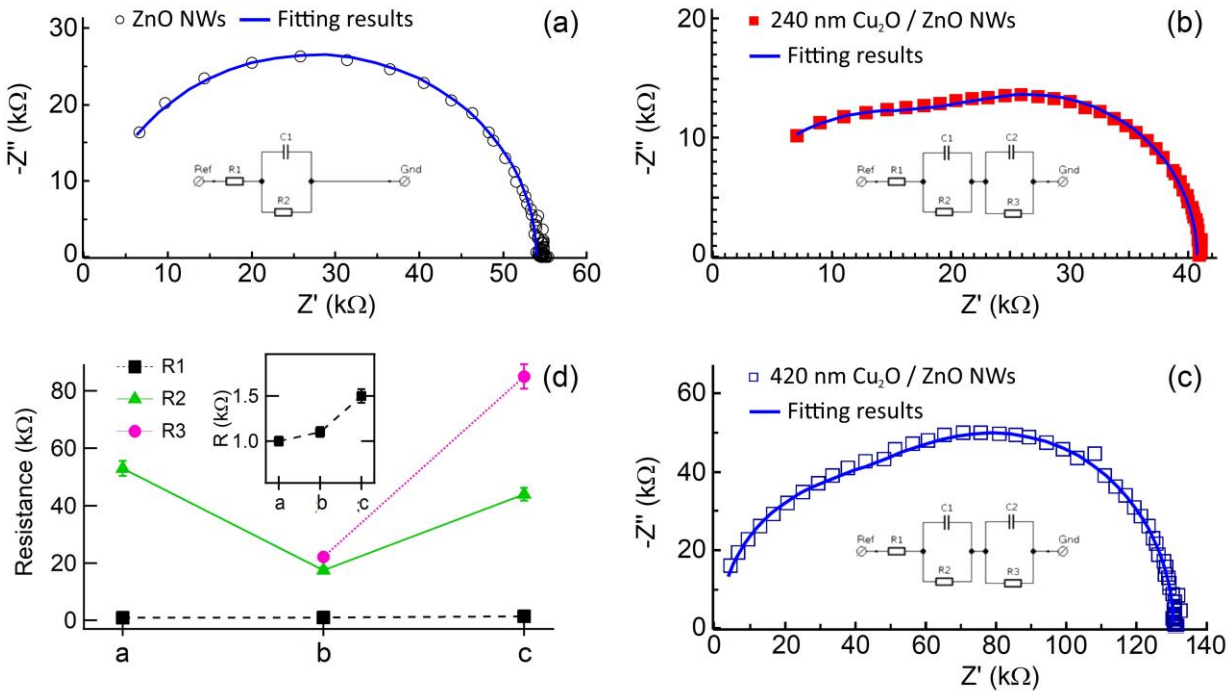

Fig. 5. Cole-Cole plot of (a) ZnO NWs, (b) ZnO-Cu_2O 240 nm, (c) ZnO-Cu_2O 420 nm, in dark, with the simulated equivalent circuit reported on each graph. (d) Resistance values obtained from the equivalent circuit simulation, for the three different samples are reported (in the inset, the series resistance R_1).

The IS spectrum in Fig. 5b-c shows an evident deviation from a single semi-circle and the data were simulated with an extra RC pair in the equivalent circuit which takes into account the additional ZnO-Cu_2O junction (R_3 and C_2 in the second RC pair are related to the ZnO-Cu_2O junction).

The series resistance values (inset of Fig. 5d), obtained by the simulated equivalent circuit, resulted to be 1 KΩ for sample a (bare ZnO NWs), 1.1 kΩ for sample c (ZnO-Cu_2O 240 nm), and 1.5 kΩ for sample d (ZnO-Cu_2O 420 nm). As we already pointed out, a compromise between the absorbing layer thickness and the low series resistance value is necessary in order to have a good transfer and collection of the photogenerated charge. According to our study, the best results are obtained with a Cu_2O layer of 240 nm.

4. Conclusions

In this work, we proposed a new fast and high-performance all-oxide photodetector based on a ZnO-Cu_2O core-shell nanowire structure. We demonstrated that the presence of a p-n rectifying junction induced a depletion region at the interface of the junction, which is able to improve the functionality of the photodetector by significantly fastening the rise and recovery time, compared to the bare ZnO NW configuration. In addition, the presence of a low bandgap absorbing layer enables photodetection in the full UV and visible range, with a record response time for this kind of oxide-based devices. Due to the low hole mobility in the p-type layer, the thickness of the Cu_2O has to be optimized (240±10 nm is the

optimum thickness in this study), searching for a compromise between light absorption and charge transport, to maximize the functionality of the device.

Moreover, core-shell structure allows faster charge-transfer due to the thinner p-type region the hole is forced to go through, before being collected at the back electrode.

We demonstrated the advantage of a core-shell structure compared to other geometries, in which NWs are embedded in a continuous thick film. The outstanding optoelectronic properties demonstrated by our device suggest an effective strategy to improve functionality also in other related fields, in which earth abundant oxides are applied, like, for instance, NW oxide solar cells.

Acknowledgements

A.V. acknowledges Knut & Alice Wallenberg Foundation, the Swedish Foundations Consolidator Fellowship, LTU Labfund program and Kempe Foundation for partial funding, and the European Union's Horizon 2020 research and innovation programme under grant agreement No 654002. I.C. acknowledges the European Commission and VINNOVA for partial support through a VINNMER Marie Curie fellowship (project Light Energy, 2015-01513). F.R. and N.A. acknowledge the Carl Trygger Foundation. A.L.P and G.M. thank the University of Catania for financial support within the "Piano della Ricerca di Ateneo 2016-2018".

References

[1] M. Deo, S. Mujawar, O. Game, A. Yengantiwar, A. Banpurkar, S. Kulkarni, J. Jog, S. Ogale, Strong photo-response in a flip-chip nanowire p-Cu2O/n-ZnO junction, Nanoscale. 3 (2011) 4706. doi:10.1039/c1nr10665a.

[2] P. Lin, X. Chen, X. Yan, Z. Zhang, H. Yuan, P. Li, Y. Zhao, Y. Zhang, Enhanced photoresponse of Cu2O/ZnO heterojunction with piezo-modulated interface engineering, Nano Res. 7 (2014) 860–868. doi:10.1007/s12274-014-0447-6.

[3] S. Rühle, A.Y. Anderson, H.N. Barad, B. Kupfer, Y. Bouhadana, E. Rosh-Hodesh, A. Zaban, All-oxide photovoltaics, J. Phys. Chem. Lett. 3 (2012) 3755–3764. doi:10.1021/jz3017039.

[4] A. Vomiero, I. Concina, E. Comini, C. Soldano, M. Ferroni, G. Faglia, G. Sberveglieri, One-dimensional nanostructured oxides for thermoelectric applications and excitonic solar cells, Nano Energy. 1 (2012) 372–390. doi:10.1016/j.nanoen.2012.02.012.

[5] Z. Dong, X. Lai, J.E. Halpert, N. Yang, L. Yi, J. Zhai, D. Wang, Z. Tang, L. Jiang, Accurate control of multishelled ZnO hollow microspheres for dye-sensitized solar cells with high efficiency, Adv. Mater. 24 (2012) 1046–1049. doi:10.1002/adma.201104626.

[6] J. Qi, X. Lai, J. Wang, H. Tang, H. Ren, Y. Yang, Q. Jin, L. Zhang, R. Yu, G. Ma, Z. Su, H. Zhao,

D. Wang, Multi-shelled hollow micro-/nanostructures, Chem. Soc. Rev. 44 (2015) 6749–6773. doi:10.1039/C5CS00344J.

[7] E. Comini, Metal oxide nano-crystals for gas sensing, Anal. Chim. Acta. 568 (2006) 28–40. doi:10.1016/j.aca.2005.10.069.

[8] E. Comini, M. Ferroni, V. Guidi, A. Vomiero, P.G. Merli, V. Morandi, M. Sacerdoti, G. Della Mea, G. Sberveglieri, Effects of Ta/Nb-doping on titania-based thin films for gas-sensing, Sensors Actuators, B Chem. 108 (2005) 21–28. doi:10.1016/j.snb.2004.10.041.

[9] G. Sberveglieri, C. Baratto, E. Comini, G. Faglia, M. Ferroni, M. Pardo, A. Ponzoni, A. Vomiero, Semiconducting tin oxide nanowires and thin films for Chemical Warfare Agents detection, Thin Solid Films. 517 (2009) 6156–6160. doi:10.1016/j.tsf.2009.04.004.

[10] T. Jiang, T. Xie, L. Chen, Z. Fu, D. Wang, Carrier concentration-dependent electron transfer in Cu2O/ZnO nanorod arrays and their photocatalytic performance, Nanoscale. 5 (2013) 2938. doi:10.1039/c3nr34219k.

[11] Z. He, Y. Xia, B. Tang, X. Jiang, J. Su, Fabrication and photocatalytic property of ZnO/Cu2O core-shell nanocomposites, Mater. Lett. 184 (2016) 148–151. doi:10.1016/j.matlet.2016.08.020.

[12] M. Ni, M.K.H. Leung, D.Y.C. Leung, K. Sumathy, A review and recent developments in photocatalytic water-splitting using TiO2 for hydrogen production, Renew. Sustain. Energy Rev. 11 (2007) 401–425. doi:10.1016/j.rser.2005.01.009.

[13] J. Wang, H. Tang, H. Wang, R. Yu, D. Wang, Multi-shelled hollow micro-/nanostructures: promising platforms for lithium-ion batteries, Mater. Chem. Front. 1 (2017) 414–430. doi:10.1039/C6QM00273K.

[14] I. Concina, Z.H. Ibupoto, A. Vomiero, Semiconducting Metal Oxide Nanostructures for Water Splitting and Photovoltaics, Adv. Energy Mater. 1700706 (2017) 1700706. doi:10.1002/aenm.201700706.

[15] I. Concina, A. Vomiero, Metal oxide semiconductors for dye- and quantum-dot-sensitized solar cells, Small. 11 (2015) 1744–1774. doi:10.1002/smll.201402334.

[16] E. Comini, C. Baratto, G. Faglia, M. Ferroni, A. Vomiero, G. Sberveglieri, Quasi-one dimensional metal oxide semiconductors: Preparation, characterization and application as chemical sensors, Prog. Mater. Sci. 54 (2009) 1–67. doi:10.1016/j.pmatsci.2008.06.003.

[17] L.L. Tian Wei, Wang Yidan, Chen Liang, Self-Powered Nanoscale Photodetectors, 1701848 (2017) 1–22. doi:10.1002/smll.201701848.

[18] J. Ding, H. Fang, Z. Lian, J. Li, Q. Lv, L. Wang, A self-powered photodetector based on a CH3NH3PbI3 single crystal with asymmetric electrodes, CrystEngComm. 18 (2016) 4405–4411. doi:10.1039/C5CE02531A.

[19] X. Wan, Y. Xu, H. Guo, K. Shehzad, A. Ali, Y. Liu, J. Yang, D. Dai, C. Lin, L. Liu, H. Cheng, F. Wang, X. Wang, H. Lu, W. Hu, X. Pi, Y. Dan, J. Luo, OPEN A self-powered high-performance graphene / silicon ultraviolet photodetector with ultra-shallow junction : breaking the limit of silicon ?, 2D Mater. Appl. 4 (2017) 1–8. doi:10.1038/s41699-017-0008-4.

[20] J. Li, S. Yuan, G. Tang, G. Li, D. Liu, J. Li, X. Hu, Y. Liu, J. Li, Z. Yang, S.F. Liu, Z. Liu, F. Gao, F. Yan, High-Performance , Self-Powered Photodetectors Based on Perovskite and Graphene, ACS Appl. Mater. Interfaces. 9 (2017) 42779–42787.

[21] C. Cheng, J. Zhan, Y. Liao, T. Lin, Y. Hsieh, junctions Self-powered and broadband photodetectors based on graphene / ZnO / silicon triple junctions, Appl. Phys. Lett. 109 (2016) 053501.

[22] L. Guo, M. Zhao, D.M. Zhuang, M.J. Cao, L. Ouyang, X. Li, R. Sun, Z. Gao, Influences of CuO phase on electrical and optical performance of Cu2O films prepared by middle frequency magnetron sputtering, Appl. Surf. Sci. 359 (2015) 36–40. doi:10.1016/j.apsusc.2015.09.216.

[23] L. Su, H.Y. Li, Y. Wang, S.Y. Kuang, Z.L. Wang, G. Zhu, Coupling of photoelectric and triboelectric effects as an effective approach for PZT-based high-performance self-powered ultraviolet photodetector, Nano Energy. 31 (2017) 264–269. doi:10.1016/j.nanoen.2016.11.019.

[24] X.X. Yu, H. Yin, H.X. Li, W. Zhang, H. Zhao, C. Li, M.Q. Zhu, Piezo-phototronic effect modulated self-powered UV/visible/near-infrared photodetectors based on CdS:P3HT microwires, Nano Energy. 34 (2017) 155–163. doi:10.1016/j.nanoen.2017.02.033.

[25] Z. Bai, X. Yan, X. Chen, H. Liu, Y. Shen, Y. Zhang, ZnO nanowire array ultraviolet photodetectors with self-powered properties, Curr. Appl. Phys. 13 (2013) 165–169. doi:10.1016/j.cap.2012.07.005.

[26] P. Lv, L. Lin, W. Zheng, M. Zheng, F. Lai, Optik Photosensitivity of ZnO / Cu 2 O thin film heterojunction, 124 (2013) 2654–2657. doi:10.1016/j.ijleo.2012.07.040.

[27] P. Lv, W. Zheng, L. Lin, F. Peng, Z. Huang, F. Lai, I – V characteristics of ZnO / Cu 2 O thin film n – i – p heterojunction, 406 (2011) 1253–1257. doi:10.1016/j.physb.2011.01.010.

[28] N.H. Ke, L.T.T. Trinh, P.K. Phung, P.T.K. Loan, D.A. Tuan, N.H. Truong, C.V. Tran, L.V.T. Hung, Changing the thickness of two layers: i-ZnO nanorods, p-Cu2O and its influence on the carriers transport mechanism of the p-Cu2O/i-ZnO nanorods/n-IGZO heterojunction, Springerplus. 5 (2016). doi:10.1186/s40064-016-2468-y.

[29] A. Vomiero, I. Concina, M.M. Natile, E. Comini, G. Faglia, M. Ferroni, I. Kholmanov, G. Sberveglieri, ZnO/ TiO2 nanonetwork as efficient photoanode in excitonic solar cells, Appl. Phys. Lett. 95 (2009). doi:10.1063/1.3257370.

[30] P. Docampo, A. Ivaturi, R. Gunning, S. Diefenbach, J. Kirkpatrick, C.M. Palumbiny, V. Sivaram,

H. Geaney, L. Schmidt-Mende, M.E. Welland, H.J. Snaith, The influence of 1D, meso- and crystal structures on charge transport and recombination in solid-state dye-sensitized solar cells, J. Mater. Chem. A. 1 (2013) 12088. doi:10.1039/c3ta11855j.

[31] P. Barthelemy, J. Bertolotti, D.S. Wiersma, A Lévy flight for light, Nature. 453 (2008) 495–498. doi:10.1038/nature06948.

[32] P. Krogstrup, H.I. Jørgensen, M. Heiss, O. Demichel, J. V. Holm, M. Aagesen, J. Nygard, A. Fontcuberta I Morral, Single-nanowire solar cells beyond the Shockley-Queisser limit, Nat. Photonics. 7 (2013) 306–310. doi:10.1038/nphoton.2013.32.

[33] L. Shen, E.Y.B. Pun, J.C. Ho, Recent developments in III–V semiconducting nanowires for high-performance photodetectors, Mater. Chem. Front. 1 (2017) 630–645. doi:10.1039/C6QM00279J.

[34] L. Vayssieres, Growth of arrayed nanorods and nanowires of ZnO from aqueous solutions, Adv. Mater. 15 (2003) 464–466. doi:10.1002/adma.200390108.

[35] L. Kumar Jangir, Y. Kumari, A. Kumar, M. Kumar, K. Awasthi, Investigation of luminescence and structural properties of ZnO nanoparticles, synthesized with different precursors, Mater. Chem. Front. 1 (2017) 1413–1421. doi:10.1039/C7QM00058H.

[36] O. Game, U. Singh, T. Kumari, A. Banpurkar, S. Ogale, ZnO(N)–Spiro-MeOTAD hybrid photodiode: an efficient self-powered fast-response UV (visible) photosensor, Nanoscale. 6 (2014) 503–513. doi:10.1039/C3NR04727J.

[37] M. Willander, O. Nur, J.R. Sadaf, M.I. Qadir, S. Zaman, A. Zainelabdin, N. Bano, I. Hussain, Luminescence from zinc oxide nanostructures and polymers and their hybrid devices, Materials (Basel). 3 (2010) 2643–2667. doi:10.3390/ma3042643.

[38] H. Makhlouf, M. Weber, O. Messaoudi, S. Tingry, M. Moret, O. Briot, R. Chtoutou, M. Bechelany, Study of Cu2O\ZnO nanowires heterojunction designed by combining electrodeposition and atomic layer deposition, Appl. Surf. Sci. 426 (2017) 301–306. doi:10.1016/j.apsusc.2017.07.130.

[39] L.C. Chen, Review of preparation and optoelectronic characteristics BN of Cu2O-based solar cells with nanostructure, Mater. Sci. Semicond. Process. 16 (2013) 1172–1185. doi:10.1016/j.mssp.2012.12.028.

[40] J. Cui, U.J. Gibson, A simple two-step electrodeposition of Cu2O/ZnO Nanopillar solar cells, J. Phys. Chem. C. 114 (2010) 6408–6412. doi:10.1021/jp1004314.

[41] Y.H. Ok, K.R. Lee, B.O. Jung, Y.H. Kwon, H.K. Cho, All oxide ultraviolet photodetectors based on a p-Cu2O film/n-ZnO heterostructure nanowires, Thin Solid Films. 570 (2014) 282–287. doi:10.1016/j.tsf.2014.05.026.

[42] M. Izaki, T. Ohta, M. Kondo, T. Takahashi, F.B. Mohamad, M. Zamzuri, J. Sasano, T. Shinagawa,

T. Pauporté, Electrodeposited ZnO-nanowire/Cu2O photovoltaic device with highly resistive ZnO intermediate layer, ACS Appl. Mater. Interfaces. 6 (2014) 13461–13469. doi:10.1021/am502246j.

[43] Z. Duan, A. Du Pasquier, Y. Lu, Y. Xu, E. Garfunkel, Effects of Mg composition on open circuit voltage of Cu2OMgxZn1-xO heterojunction solar cells, Sol. Energy Mater. Sol. Cells. 96 (2012) 292–297. doi:10.1016/j.solmat.2011.09.047.

[44] B. Kramm, A. Laufer, D. Reppin, A. Kronenberger, P. Hering, A. Polity, B.K. Meyer, The band alignment of Cu2O/ZnO and Cu2O/GaN heterostructures, Appl. Phys. Lett. 100 (2012). doi:10.1063/1.3685719.

[45] S.S. Wilson, J.P. Bosco, Y. Tolstova, D.O. Scanlon, G.W. Watson, H.A. Atwater, Interface stoichiometry control to improve device voltage and modify band alignment in ZnO/Cu $_2$ O heterojunction solar cells, Energy Environ. Sci. 7 (2014) 3606–3610. doi:10.1039/C4EE01956C.

[46] A. Escobedo Morales, E. Sánchez Mora, U. Pal, Use of diffuse reflectance spectroscopy for optical characterization of un-supported nanostructures, Rev. Mex. Física S. 53 (2007) 18–22. http://www.researchgate.net/publication/229050010_Use_of_diffuse_reflectance_spectroscopy_for_optical_characterization_of_un-supported_nanostructures/file/79e41507eead49bb27.pdf.

[47] G.G. Condorelli, G. Malandrino, I. Fragala, Metal-Organic Chemical Vapor Deposition of Copper and Copper(I) Oxide: Kinetics and Reaction Mechanisms in the Presence of Oxygen, Chem. Mater. 7 (1995) 2096–2103. doi:10.1021/cm00059a017.

[48] G.G. Condorelli, G. Malandrino, I. Fragalà, Metal–Organic Chemical Vapor Deposition of Copper-Containing Phases: Kinetics and Reaction Mechanisms, Chem. Mater. 6 (1994) 1861–1866. doi:10.1021/cm00046a048.

[49] C.L. Kuo, T.J. Kuo, M.H. Huang, Hydrothermal synthesis of ZnO microspheres and hexagonal microrods with sheetlike and platelike nanostructures, J. Phys. Chem. B. 109 (2005) 20115–20121. doi:10.1021/jp0528919.

[50] H. Lahmar, A. Azizi, G. Schmerber, A. Dinia, Effect of the thickness of the ZnO buffer layer on the properties of electrodeposited p-Cu $_2$ O/n-ZnO/n-AZO heterojunctions, RSC Adv. 6 (2016) 68663–68674. doi:10.1039/C6RA04834J.

[51] Z. Bai, Y. Zhang, Self-powered UV-visible photodetectors based on ZnO/Cu2O nanowire/electrolyte heterojunctions, J. Alloys Compd. 675 (2016) 325–330. doi:10.1016/j.jallcom.2016.03.051.

[52] X. Li, C. Gao, H. Duan, B. Lu, X. Pan, E. Xie, Nanocrystalline TiO 2 film based photoelectrochemical cell as self-powered UV-photodetector, Nano Energy. 1 (2012) 640–645. doi:10.1016/j.nanoen.2012.05.003.

[53] C. Gao, X. Li, Y. Wang, L. Chen, X. Pan, Z. Zhang, E. Xie, Titanium dioxide coated zinc oxide

nanostrawberry aggregates for dye-sensitized solar cell and self-powered UV-photodetector, J. Power Sources. 239 (2013) 458–465. doi:10.1016/j.jpowsour.2013.04.003.

[54] C. Gao, X. Li, X. Zhu, L. Chen, Y. Wang, F. Teng, Z. Zhang, H. Duan, E. Xie, High performance, self-powered UV-photodetector based on ultrathin, transparent, SnO2-TiO2 core-shell electrodes, J. Alloys Compd. 616 (2014) 510–515. doi:10.1016/j.jallcom.2014.07.171.

[55] Y. Li, Z. Zhang, W. Han, C. Jiang, E. Xie, Analysis on the piezotronic effect in a strained piezo-Schottky junction with AC impedance spectroscopy, Nano Energy. 36 (2017) 118–125. doi:10.1016/j.nanoen.2017.04.021.